

# Training Adversarial Discriminators for Cross-channel Abnormal Event Detection in Crowds

Mahdyar Ravanbakhsh  
DITEN, University of Genova  
mahdyar.ravan@ginevra.dibe.unige.it

Moin Nabi  
DISI, University of Trento  
moin.nabi@unitn.it

Enver Sangineto  
DISI, University of Trento  
enver.sangineto@unitn.it

Nicu Sebe  
DISI, University of Trento  
sebe@disi.unitn.it

## ABSTRACT

Abnormal crowd behaviour detection attracts a large interest due to its importance in video surveillance scenarios. However, the ambiguity and the lack of sufficient *abnormal* ground truth data makes end-to-end training of large deep networks hard in this domain. In this paper we propose to use Generative Adversarial Nets (GANs), which are trained to generate only the *normal* distribution of the data. During the adversarial GAN training, a discriminator ( $D$ ) is used as a supervisor for the generator network ( $G$ ) and vice versa. At testing time we use  $D$  to solve our *discriminative* task (abnormality detection), where  $D$  has been trained without the need of manually-annotated abnormal data. Moreover, in order to prevent  $G$  learn a trivial identity function, we use a cross-channel approach, forcing  $G$  to transform raw-pixel data in motion information and vice versa. The quantitative results on standard benchmarks show that our method outperforms previous state-of-the-art methods in both the frame-level and the pixel-level evaluation.

## KEYWORDS

Generative Adversarial Networks, Abnormality Detection, Crowd behaviour Analysis

## 1 INTRODUCTION

Detecting abnormal crowd behaviour is motivated by the increasing interest in video-surveillance systems for public safety. However, despite a lot of research has been done in this area in the past years [2, 6–10, 19], the problem is still open.

One of the main reasons for which abnormality detection is challenging is the relatively small size of the existing datasets with ground truth abnormality. In order to deal with this problem, most of the existing abnormality-detection methods focus on learning only the *normal* pattern of the crowd, for which only weakly annotated training data are necessary (e.g., videos representing only the normal crowd behaviour in a given scene). Detection is then performed by measuring the difference of the test frame representation with respect to the learned normal pattern (e.g., using a one-class SVM).

However, the lack of sufficiently large datasets provided with abnormality ground truth makes it hard to train modern deep networks which are based on a fully-supervised training protocol (e.g., using a classification task).

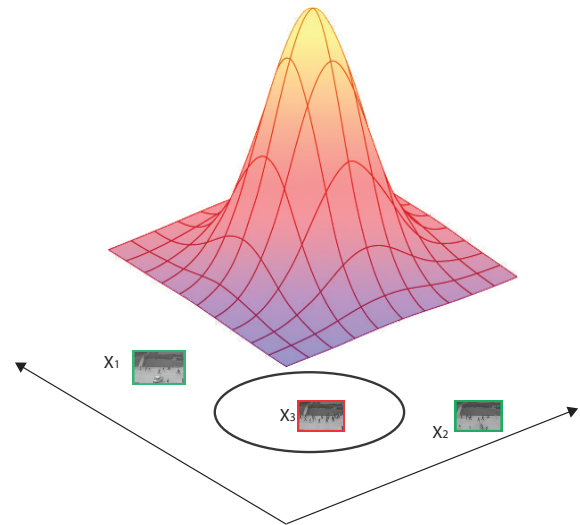


**Figure 1: A schematic representation of our Adversarial Discriminator. The data distribution (represented by the Gaussian curve on the top) is denser in the feature space area corresponding to the only real and “normal” data observed by  $G$  and  $D$  during training.  $D$  learns to separate this area from the rest of the feature space. In the figure, the black circle represents the decision boundary learned by  $D$ . Outside this boundary lie both non-realistically generated images (e.g.,  $x_2$ ) and real but non-normal images (e.g.,  $x_1$ ). At testing time we exploit the learned decision boundary in order to detect abnormal events in new images.**

In this paper we propose to solve the abnormality detection problem using Generative Adversarial Networks (GANs) [3]. GANs are deep networks commonly used to generate data (e.g., images) and are trained using only unsupervised data. The supervisory information in a GAN is indirectly provided by an adversarial game between two independent networks: a generator ( $G$ ) and a discriminator ( $D$ ). During training,  $G$  generates new data and  $D$  tries to understand whether its input is real (i.e., it is a training image) or it was generated by  $G$ . This competition between  $G$  and  $D$  is helpful in boosting the ability of both  $G$  and  $D$ . At testing time, only  $G$  is used to generate new data.

We use this framework to train our  $G$  and  $D$  using as training data only frames of videos without abnormality. Doing so,  $G$  learns

how to generate *only* the normal pattern of the observed scene. On the other hand,  $D$  learns how to distinguish what is normal from what is not, because abnormal events are considered as outliers with respect to the data distribution (see Fig. 1). Since our final goal is a discriminative task (at testing time we need to detect possible anomalies in a new scene), different from common GAN-based approaches, we propose to directly use  $D$  after training. The advantage of this approach is that we do not need to train one-class SVMs or other classifiers on top of the learned visual representations and we present one of the very first deep learning approaches for abnormality detection which can be trained end-to-end.

As far as we know, the only other end-to-end deep learning framework for abnormality detection is the recently proposed approach of Hasan et al. [4]. In [4] a Convolutional Autoencoder is used to learn the crowd-behaviour normal pattern and used at testing time to *generate* the normal scene appearance, using the reconstruction error to measure an abnormality score. The main difference of our approach with [4] is that we exploit the adversary game between  $G$  and  $D$  to simultaneously approximate the normal data distribution and train the final classifier. In Sec. 6-7 we compare our method with both [4] and a strong baseline in which we use the reconstruction error of our generator  $G$ . Similarly to [4], in [21] Stacked Denoising Autoencoders are used to reconstruct the input image and learn task-specific features using a deep network. However, in [21] the final classifier is a one-class SVM which is trained on top of the learned representations and it is not jointly optimized together with the deep-network-based features. Moreover, a model of the noise need to be manually provided to train the Denoising Autoencoders, and understanding what is the most effective noise model is not easy in an unsupervised setting.

The second novelty we propose in this paper is a *multi-channel* and a *cross-channel* data representation. Specifically, we use both appearance and motion (optical flow) information: a two-channel approach which has been proved to be empirically important in previous work on abnormality detection [9, 15, 21]. Moreover, we propose to use a cross-channel approach where, inspired by [5], we train two networks which respectively transform raw-pixel images in optical-flow representations and vice versa. The rationale behind this is that the architecture of our conditional generators  $G$  is based on an encoder-decoder (see Sec. 3) and we use these channel-transformation tasks in order to prevent  $G$  learn a trivial identity function and force  $G$  and  $D$  to construct sufficiently informative internal representations. In Sec. 7 we compare the cross-channel tasks with two corresponding same-channel tasks. Even if the latter achieve surprisingly good results, the cross-channel training strategy largely outperforms the training protocol with no image transformations.

Extensive experiments on the most common anomaly detection benchmarks show a large accuracy margin of the proposed approach compared to the previous state of the art.

In summary, our contributions are:

- As far as we know, our proposal is the first using GANs for a discriminative task, directly exploiting the discriminator trained using the commonly adopted adversarial game.
- We propose multi-channel and cross-channel generative tasks which are used to learn informative representations of the normal pattern of a scene.
- Our method outperforms all the previous work tested in the most common abnormality detection benchmarks using all the common evaluation protocols.

In the rest of this paper we review the related literature in Sec. 2 and we present our method in Sec. 3-5. Experimental results are reported in Sec. 6-7. Finally, we show some qualitative results in Sec. 8 and we conclude in Sec. 9.

## 2 RELATED WORK

In this section we briefly review previous work considering: (1) our application scenario (Abnormality Detection) and (2) our methodology based on GANs.

**Abnormality Detection** There is a wealth of literature on abnormality detection [2, 6, 8–11, 19]. Most of the previous work is based on hand-crafted features (e.g., Optical-Flow, Tracklets, etc.) to model the normal activity patterns, whereas our method learns features from raw-pixels using a deep-learning based approach using an end-to-end training protocol. Deep learning has also been investigated for abnormality detection tasks in [15, 17, 18]. Nevertheless, these works mainly use existing CNN models trained for other tasks (e.g., object recognition) which are adapted to the abnormality detection task. For instance, Ravanbakhsh et al. [15] propose a Binary Quantization Layer plugged as a final layer on top of a CNN, which represents temporal motion patterns for the task of abnormality segmentation. However, their network is not trained end-to-end and is based on a complex post-processing stage and on a pre-computed codebook of the convolutional feature map values. Similarly, in [17, 18], a fully convolutional neural network is proposed which is a combination of a pre-trained CNN (i.e., AlexNet) and a new convolutional layer where kernels have been trained from scratch.

Sabokrou et al. [16] introduce a patch-based anomaly detection framework based on the Autoencoder (AE) reconstruction error and sparsity constraints. However this work is limited to a single modality setup. Stacked Denoising Autoencoders (SDAs) are used by Xu et al. [21] to learn motion and appearance feature representations. The networks used in this work are relatively shallow, since training deep SDAs on small abnormality datasets can be prone to over-fitting issues and the networks' input is limited to a small image patch. Moreover, after the SDAs-based features have been learned, multiple one-class SVMs need to be trained on top of these features in order to create the final classifiers, and the learned features may be sub-optimal because they are not jointly optimized with respect to the final abnormality discrimination task. The only deep learning based approach proposing a framework which can be trained in an end-to-end fashion we are aware of is the Convolutional AE network proposed in [4], where a deep representation is learned by minimizing the AE-based frame reconstruction. At testing time, an anomaly is detected computing the difference between the AE-based frame reconstruction and the real test frame. We compare with this work in Sec. 6 and in Sec. 7 we present a modified version of our GAN-based approach in which

we use the reconstruction errors of our GAN-trained generators using a detection strategy similar to [4].

**GANs** [3, 5, 13, 14, 20] are based on a two-player game between two different networks, both trained with unsupervised data. One network is the *generator* ( $G$ ), which aims at generating realistic data (e.g., images). The second network is the *discriminator* ( $D$ ), which aims at discriminating real data from data generated from  $G$ . Specifically, the *conditional* GANs [3], that we use in our approach, take as input an image  $x$  and generate a new image  $r$ .  $D$  tries to distinguish  $x$  from  $r$ , while  $G$  tries to “fool”  $D$  producing more and more realistic images which are hard to be distinguished. Very recently Isola et al. [5] proposed an “image-to-image translation” framework based on conditional GANs, where both the generator and the discriminator are conditioned on the real data. They show that a “U-Net” encoder-decoder with skip connections can be used as the generator architecture together with a patch-based discriminator in order to transform images with respect to different representations. We adopt this framework in order to generate optical-flow images from raw-pixel frames and vice versa. However, we do not aim at generating image representations which look realistic, but we use  $G$  to learn the normal pattern of an observed crowd scene. At testing time,  $D$  is directly used to detect abnormal areas using the appearance and the motion information of the input frame.

### 3 CROSS-CHANNEL GENERATION TASKS

We use the framework proposed by Isola et al. [5] to learn the normal behaviour of the observed scene. We use two channels: appearance (i.e., raw-pixels) and motion (optical flow images) and two cross-channel tasks. In the first task, we generate optical-flow images starting from the original frames, while in the second task we generate appearance information starting from an optical flow image.

Specifically, let  $F_t$  be the  $t$ -th frame of a training video and  $O_t$  the optical flow obtained using  $F_t$  and  $F_{t+1}$ .  $O_t$  is computed using [1]. We train two networks:  $\mathcal{N}^{F \rightarrow O}$ , which generates optical-flow from frames (task 1) and  $\mathcal{N}^{O \rightarrow F}$ , which generates frames from optical-flow (task 2). In both cases, inspired by [5], our networks are composed of a conditional generator  $G$  and a conditional discriminator  $D$ .  $G$  takes as input an image  $x$  and a noise vector  $z$  (drawn from a noise distribution  $\mathcal{Z}$ ) and outputs an image  $r = G(x, z)$  of the same dimensions of  $x$  but represented in a different channel. For instance, in case of  $\mathcal{N}^{F \rightarrow O}$ ,  $x$  is a frame ( $x = F_t$ ) and  $r$  is the *reconstruction* of its corresponding optical-flow image  $y = O_t$ . On the other hand,  $D$  takes as input two images  $x$  and  $u$  (where  $u$  is either  $y$  or  $r$ ) and outputs a scalar representing the probability that both its input images came from the real data.

Both  $G$  and  $D$  are fully-convolutional networks, composed of convolutional layers, batch-normalization layers and ReLU nonlinearities. In case of  $G$  we adopt the U-Net architecture [5], which is an encoder-decoder, where the input  $x$  is passed through a series of progressively downsampling layers until a bottleneck layer, at which point the forwarded information is upsampled. Downsampling and upsampling layers in a symmetric position with respect to the bottleneck layer are connected by *skip connections* which help preserving important local information. The noise vector  $z$  is implicitly provided to  $G$  using dropout, applied to multiple layers.

The two input images  $x$  and  $u$  of  $D$  are concatenated and passed through 5 convolutional layers. In more detail,  $F_t$  is represented using the standard RGB representation, while  $O_t$  is represented using the horizontal, the vertical and the magnitude components. Thus, in both tasks, the input of  $D$  is composed of 6 components, whose relative order depends on the specific task. All the images are rescaled to  $256 \times 256$ . We use the *PatchGAN* discriminator proposed in [5], which is based on a “small” fully-convolutional discriminator  $\hat{D}$ .  $\hat{D}$  is applied to a  $30 \times 30$  grid, where each position of the grid corresponds to a  $70 \times 70$  patch  $p_x$  in  $x$  and a corresponding patch  $p_u$  in  $u$ . The output of  $\hat{D}$  is a score representing the probability that  $p_x$  and  $p_u$  are either both real or  $p_u$  was generated from  $p_x$ . During training, the output of  $\hat{D}$  over all the grid positions is averaged and this provides the final score of  $D$  with respect to  $x$  and  $u$ . Conversely, at testing time we directly use  $\hat{D}$  as a “detector” which is run over the grid to spatially localize the possible abnormal regions in the input frame (see Sec. 5). We refer to [5] for the architectural details of  $G$  and  $\hat{D}$ .

### 4 TRAINING

$G$  and  $D$  are trained using both a conditional GAN loss  $\mathcal{L}_{cGAN}$  and a reconstruction loss  $\mathcal{L}_{L1}$ . In case of  $\mathcal{N}^{F \rightarrow O}$ , the training set is composed of pairs of frame-optical flow images  $\mathcal{X} = \{(F_t, O_t)\}_{t=1, \dots, N}$ .  $\mathcal{L}_{L1}$  is given by:

$$\mathcal{L}_{L1}(x, y) = \|y - G(x, z)\|_1, \quad (1)$$

where  $x = F_t$  and  $y = O_t$ , while the conditional adversarial loss  $\mathcal{L}_{cGAN}$  is:

$$\mathcal{L}_{cGAN}(G, D) = \mathbb{E}_{(x, y) \in \mathcal{X}} [\log D(x, y)] + \quad (2)$$

$$\mathbb{E}_{x \in \{F_t\}, z \in \mathcal{Z}} [\log(1 - D(x, G(x, z)))] \quad (3)$$

Conversely, in case of  $\mathcal{N}^{O \rightarrow F}$ , we use  $\mathcal{X} = \{(O_t, F_t)\}_{t=1, \dots, N}$ . We refer to [5] for more details about the training procedure. What is important to highlight here is that both  $\{F_t\}$  and  $\{O_t\}$  are collected using the frames of the only *normal* videos of the training dataset. The fact that we do not need videos showing abnormal events at training time makes it possible to train the discriminators corresponding to our two tasks without the need of supervised training data:  $G$  acts as an implicit supervision for  $D$ .

During training the generators of the two tasks ( $G^{F \rightarrow O}$  and  $G^{O \rightarrow F}$ ) observe only normal scenes. As a consequence, after training they are not able to reconstruct an abnormal event. For instance, in Fig. 2 (first column) a frame  $F$  containing a vehicle unusually moving in a University campus is input to  $G^{F \rightarrow O}$  and in the generated optical flow image ( $r_O = G^{F \rightarrow O}(F)$ ) the abnormal area corresponding to that vehicle is not reconstructed. Similarly, when the real optical flow ( $O$ ) associated with  $F$  is input to  $G^{O \rightarrow F}$ , the network tries to reconstruct the area corresponding to the vehicle but the output is a set of unstructured blobs (Fig. 3, first column). On the other hand, the two corresponding discriminators  $D^{F \rightarrow O}$  and  $D^{O \rightarrow F}$  during training have learned to distinguish what is plausibly real from what is not.

Note that, even if a global optimum can be theoretically reached by a general GAN in which the data distribution and the generative

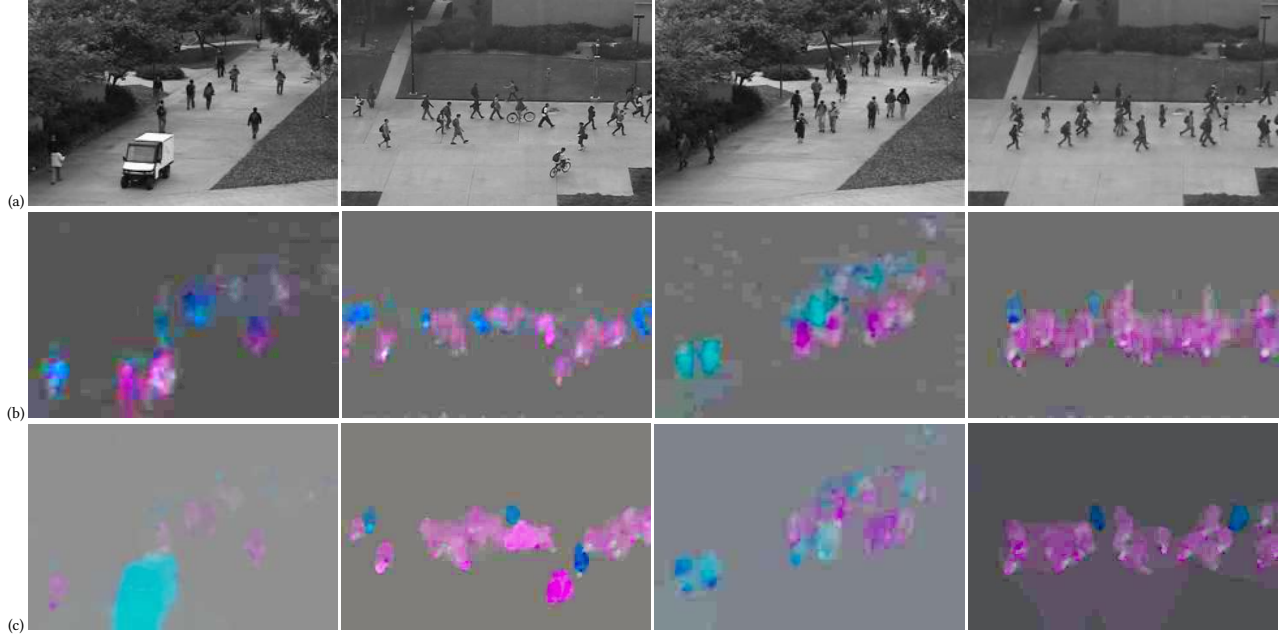


**Figure 2: A few qualitative results showing the images generated by  $G^{F \rightarrow O}$  after training is completed: (a) real frames, (b) the corresponding reconstructed optical flow, (c) the real optical flow images corresponding to (a). The first two columns represent an abnormal scene, while the other two columns depict a normal situation. Note that the motion of the vehicle in the first sample and of the bicycle in the bottom of the second sample have not been reconstructed.**

distribution totally overlap each other [3], in practice the generator is very rarely able to produce a completely realistic image. For instance, in Fig. 3 the high-resolution details of the generated pedestrians are quite smooth and the human body is approximated with a blob-like structure. As a consequence, at the end of the training process, the discriminator has learned to separate real data from artefacts. This situation is schematically represented in Fig. 1. The data distribution is depicted by the Gaussian curve on the top of the figure. The discriminator is represented by the decision boundary on the learned feature space which separates the densest area of this distributions from the rest of the space. Outside this area lie both non-realistic generated images (e.g.  $x_2$ ) and real, abnormal events (e.g.,  $x_1$ ). Our hypothesis is that the latter lie outside the discriminator’s decision boundaries because they represent situations never observed during training and hence treated by  $D$  as outliers. We use the discriminator’s learned decision boundaries in order to detect  $x_1$ -like events as explained in the next section.

## 5 ANOMALY DETECTION

At testing time only the discriminators are used. More specifically, let  $\hat{D}^{F \rightarrow O}$  and  $\hat{D}^{O \rightarrow F}$  be the patch-based discriminators trained using the two channel-transformation tasks (see Sec. 3). Given a test frame  $F$  and its corresponding optical-flow image  $O$ , we apply the two patch-based discriminators on the same  $30 \times 30$  grid used for training. This results in two  $30 \times 30$  score maps:  $S^O$  and  $S^F$  for the first and the second task, respectively. Note that we do not need to produce the reconstruction images to use the discriminators. For instance, for a given position on the grid,  $\hat{D}^{F \rightarrow O}$  takes as input

a patch  $p_F$  on  $F$  and a corresponding patch  $p_O$  on  $O$ . A possible abnormal area in  $p_F$  and/or in  $p_O$  (e.g., an unusual object or an unusual movement) corresponds to an outlier with respect to the data distribution learned by  $\hat{D}^{F \rightarrow O}$  during training and results in a low value of  $\hat{D}^{F \rightarrow O}(p_F, p_O)$ .

The two score maps are summed with equal weights:  $S = S^O + S^F$ . The values in  $S$  are normalized in the range  $[0, 1]$ . In more detail, for each test video  $V$  we compute the maximum value  $m_s$  of all the elements of  $S$  over all the input frames of  $V$ . For each frame the normalized score map is given by:

$$N(i, j) = 1/m_s S(i, j). \quad (4)$$

Finally, we upsample  $N$  to the original frame size ( $N'$ ) and we use the previously computed optical-flow information to filter out non-motion areas, obtaining the final abnormality map:

$$A(i, j) = \begin{cases} 1 - N'(i, j) & \text{if } O(i, j) > 0 \\ 0 & \text{otherwise.} \end{cases} \quad (5)$$

Note that all the post-processing steps (upsampling, normalization, motion-based filtering) are quite common strategies [21] and we do not use any hyper-parameter or ad-hoc heuristic which need to be tuned on a specific dataset.

## 6 EXPERIMENTAL RESULTS

In this section we compare the proposed method against the state of the art using common benchmarks for crowd-behaviour abnormality detection. The evaluation is performed using both a *pixel-level* and a *frame-level* protocol and the evaluation setup proposed in

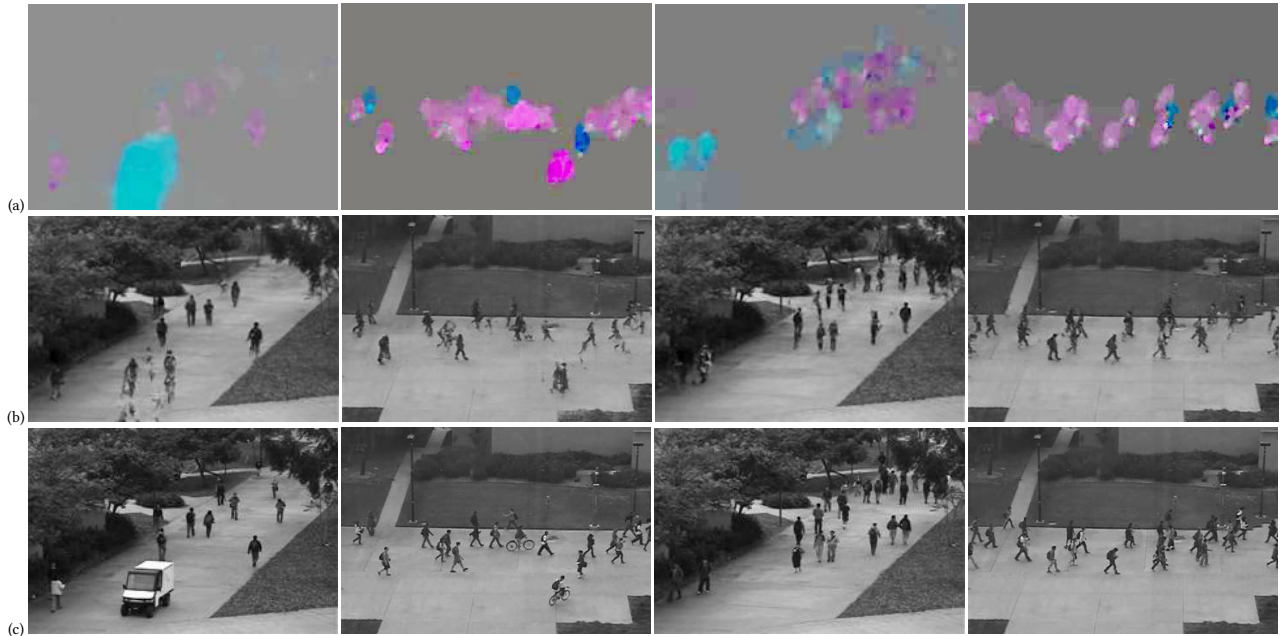


**Figure 3: Images generated by  $G^{O \rightarrow F}$  after training is completed: (a) the input optical-flow images, (b) the corresponding reconstructed frames, (c) the real frames corresponding to (a). The first two columns represent an abnormal scene, while the other two columns depict a normal situation. Note that the abnormal objects in the first two samples are completely missing in the corresponding reconstructions. In the first image (from left) there is a large moving area (produced by a car) which has not been reconstructed:  $G^{O \rightarrow F}$  simply does not know how to “draw” a car, hence the car “disappeared” from the reconstruction. Similarly, in the second image two fast moving bicycles “disappeared” from the frame reconstruction.**

[7]. The rest of this section describes the datasets, the experimental protocols and the obtained results.

**Implementation details.**  $\mathcal{N}^{F \rightarrow O}$  and  $\mathcal{N}^{O \rightarrow F}$  are trained using the training sequences of the UCSD dataset. All frames are resized to  $256 \times 256$  pixels (see Sec. 3). Training is based on stochastic gradient descent with momentum 0.5 and batch size 1. We train our networks for 10 epochs each. All the GAN-specific hyper-parameters values have been set following the suggestions in [5], while in our approach there is no dataset-specific hyper-parameter which needs to be tuned. This makes the proposed method particularly robust, especially in a weakly-supervised scenario in which ground-truth validation data with abnormal frames are not given. All the results presented in this section but ours are taken from [12, 21] which report the best results achieved by each method independently tuning the method-specific hyper-parameter values.

Full-training of one network (10 epochs) takes on average less than half an hour with 6,800 training samples. At testing time, one frame is processed in 0.18 seconds (the whole processing pipeline, optical-flow computation and post-processing included). These computational times have been computed using a single GPU (Tesla K40).

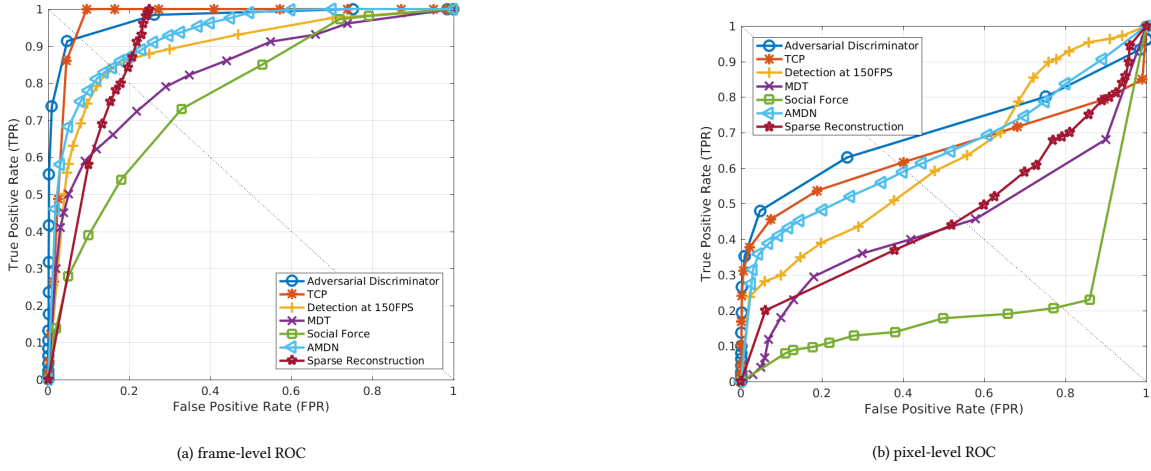
**Datasets and experimental setup.** We use two standard datasets: the UCSD Anomaly Detection Dataset [9] and the UMN Social-Force [10]. The **UCSD dataset** is split into two subsets: *Ped1*, which is composed of 34 training and 16 test sequences, and *Ped2*, which is composed of 16 training and 12 test video samples. The overall

dataset contains about 3,400 abnormal and 5,500 normal frames. This dataset is challenging due to the low resolution of the images and the presence of different types of moving objects and anomalies in the scene. The **UMN dataset** contains 11 video sequences in 3 different scenes, with a total amount of 7,700 frames. All the sequences start with a normal state and end with an abnormal frame.

**Frame-level evaluation.** In the frame-level anomaly detection evaluation protocol, an abnormality label is predicted for a given test frame if at least one abnormal pixel is predicted in that frame: In this case the abnormality label is assigned to the whole frame. This evaluation procedure is iterated using a range of confidence thresholds in order to build a corresponding ROC curve. The results are reported in Tab. 1 (UCSD dataset) and Tab. 2 (UMN dataset) using the Equal Error Rate (EER) and the Area Under Curve (AUC). Our method is called *Adversarial Discriminator*. Fig. 4 shows the ROC curves (UCSD dataset).

**Pixel-level anomaly localization.** The goal of the pixel-level evaluation is to measure the accuracy of the abnormality spatial localization. Following the protocol suggested in [7], the predicted abnormal pixels are compared with the pixel-level ground truth. A test frame is a true positive if the area of the predicted abnormal pixels overlaps with the ground-truth area by at least 40%, otherwise the frame is counted as a false positive. Fig. 4 shows the ROC curves of the localization accuracy over the USDC dataset, and EER and AUC values are reported in Tab. 1.




**Figure 4: ROC curves for Ped1 (UCSD dataset).**

Method	Ped1 (frame-level)		Ped1 (pixel-level)		Ped2 (frame-level)	
	EER	AUC	EER	AUC	EER	AUC
MPPCA [6]	40%	59.0%	81%	20.5%	30%	69.3%
Social force (SFM) [10]	31%	67.5%	79%	19.7%	42%	55.6%
SF+MPPCA [9]	32%	68.8%	71%	21.3%	36%	61.3%
Sparse Reconstruction [2]	19%	—	54%	45.3%	—	—
MDT [9]	25%	81.8%	58%	44.1%	25%	82.9%
Detection at 150fps [8]	15%	91.8%	43%	63.8%	—	—
TCP [15]	8%	95.7%	40.8%	64.5%	18%	88.4%
AMDN (double fusion) [21]	16%	92.1%	40.1%	67.2%	17%	90.8%
Convolutional AE [4]	27.9%	81%	—	—	21.7%	90%
Adversarial Discriminator	7%	<b>96.8%</b>	<b>34%</b>	<b>70.8%</b>	<b>11%</b>	<b>95.5%</b>

**Table 1: UCSD dataset. Comparison of different methods. All but our results are taken from [21].**

Method	AUC
Optical-flow [10]	0.84
Social force (SFM) [10]	0.96
Sparse Reconstruction [2]	0.97
Commotion Measure [12]	0.98
TCP [15]	0.98
Adversarial Discriminator	<b>0.99</b>

**Table 2: UMN dataset. Comparison of different methods. All but our results are taken from [12].**

**Overall evaluation.** The results in Tab. 1 and Tab. 2 show that the proposed approach *outperforms all the previous work in all the datasets and with all the evaluation protocols.*

## 7 ABLATION STUDY

In this section we analyse the main aspects of the proposed method, which are: the use of the discriminators trained by our conditional GANs as the final classifiers, the importance of the cross-channel tasks and the influence of the multiple-channel approach (i.e., the importance of fusing appearance and motion information). For this purpose we use the UCSD Ped2 dataset (frame-level evaluation) and we test different strong baselines obtained by amputating important aspects of our method.

The first baseline, called *Adversarial Generator*, is obtained using the reconstruction error of  $G^{F \rightarrow O}$  and  $G^{O \rightarrow F}$ , which are the generators trained as in Sec. 3-4. In more detail, at testing time we use  $G^{F \rightarrow O}$  and  $G^{O \rightarrow F}$  to *generate* a channel transformation of the input frame  $F$ . Let  $r_O = G^{F \rightarrow O}(F)$  and  $r_F = G^{O \rightarrow F}(O)$ , where  $O$  is the optical-flow image corresponding to  $F$ . Then, similarly to Hasan et al. [4], we compute the appearance reconstruction error using:  $e_F = |F - r_F|$  and the motion reconstruction error using:  $e_O = |O - r_O|$ . When an anomaly is present in  $F$  and/or in  $O$ ,  $G^{F \rightarrow O}$  and  $G^{O \rightarrow F}$  are not able to accurately reconstruct the corresponding

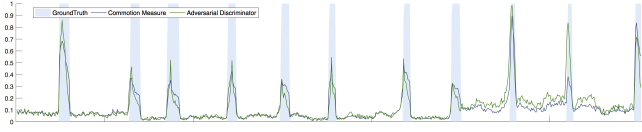


Figure 5: Visualization of the “detection signal” as proposed in [12].

area (see Sec. 8 and Fig. 2-3). Hence, we expect that in the abnormal areas of  $F$ ,  $e_F$  and/or  $e_O$  have higher values than the mean values computed using normal test frames. The final abnormality map is obtained by applying the same post-processing steps described in Sec. 5: (1) we upsample the reconstruction errors, (2) we normalize the two errors with respect to all the frames in the test video  $V$  and in each channel independently of the other channel, (3) we fuse the normalized maps and (4) we use optical-flow to filter-out non-motion areas. The only difference with respect to the corresponding post-processing stages adopted in case of *Adversarial Discriminator* and described in Sec. 5 is a weighted fusion of the channel-dependent maps by weighting the importance of  $e_O$  twice as the importance of  $e_F$ .

In the second strong baseline we do use the discriminators but we do not use a cross-channel strategy. In more detail, we train two networks  $\mathcal{N}^{F \rightarrow F}$  and  $\mathcal{N}^{O \rightarrow O}$  as described in Sec. 3-4 but we use two “same-channel” tasks, using the generators of the two networks for autoencoding tasks, similarly to [4] and [21]. Note that the noise ( $z$ ) provided by dropout (Sec. 3) acts as a form of input perturbation. At testing time we use the corresponding patch-based discriminators  $\hat{D}^{F \rightarrow F}$  and  $\hat{D}^{O \rightarrow O}$ . The rest of the pipeline (training, post-processing, etc.) is the same as in *Adversarial Discriminator*. We call this baseline *Same Channel Discriminator*.

In *Adversarial Discriminator F* we use only  $\hat{D}^{O \rightarrow F}$  and in *Adversarial Discriminator O* we use only  $\hat{D}^{F \rightarrow O}$ . These two baselines show the importance of channel-fusion.

Note that in all the baselines, including the last, we use optical-flow information (Eq. 5) to filter-out non-motion pixels and we compute pixel-level abnormality maps, which make all these weaker versions of our method suitable for pixel-level abnormality detection.

The results are shown in Tab. 3. Since the values corresponding to two performance measures (EER and AUC) are not always coherent, ranking all the baselines is difficult. However, it is clear that *Adversarial Generator* achieves a very high accuracy: Comparing *Adversarial Generator* with all the methods in Tab. 1 (except *Adversarial Discriminator*), it is the state-of-the-art approach. Conversely, the overall accuracy of *Same Channel Discriminator* drops significantly with respect to *Adversarial Discriminator*, and this shows the importance of the cross-channel tasks. However, comparing *Same Channel Discriminator* with the values in Tab. 1, also this baseline outperforms or is very close to the best performing systems on this dataset.

Finally, the worst performance was obtained by *Adversarial Discriminator F*, with values much worse than *Adversarial Discriminator O*. We believe this is due to the fact that *Adversarial Discriminator O* takes as input a real frame which contains a much more detailed information with respect to the optical-flow input

Baseline	EER	AUC
Adversarial Generator	15.6%	93.4%
Same Channel Discriminator	17%	88.7%
Adversarial Discriminator F	24.9%	81.6%
Adversarial Discriminator O	13.2%	90.1%
Adversarial Discriminator	11%	95.5%

Table 3: Results of the ablation analysis on the UCSD dataset, Ped2 (frame-level evaluation). See the text for details.

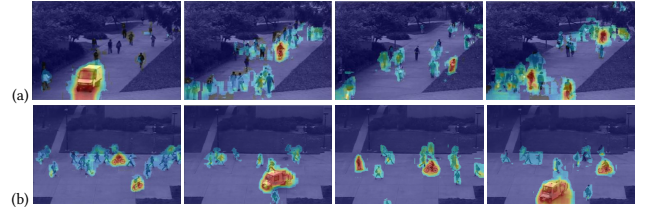


Figure 6: A few examples of pixel-level detections of our method: (a) Ped1 dataset, (b) Ped2 dataset. We adopt the standard visualization which highlights the predicted abnormal areas with a bright red colour.



Figure 7: Some examples of miss-detections of our method.

of *Adversarial Discriminator O*. However, the fusion of these two detectors is crucial in boosting the performance of the proposed method *Adversarial Discriminator*.

It is also interesting to compare our *Adversarial Generator* with the Convolutional Autoencoder proposed in [4], being both based on the reconstruction error (see Sec. 1). The results of the Convolutional Autoencoder on the same dataset are: 21.7% and 90% EER and AUC, respectively (Tab. 1), which are significantly worse than our baseline based on GANs.

## 8 QUALITATIVE RESULTS

In this section we show some qualitative results of our generators  $G^{F \rightarrow O}$  (Fig. 2) and  $G^{O \rightarrow F}$  (Fig. 3) and the detections of *Adversarial Discriminator* (Fig. 5-7).

Fig. 2-3 show that the generators are pretty good in generating normal scenes. However, high-resolution structures of the pedestrians are not accurately reproduced. This confirms that the data distribution and the generative distribution do not completely overlap each other (similar results have been observed in [5, 13, 14, 20]). On the other hand, abnormal objects or fast movements are completely missing from the reconstructions: the generators simply cannot reconstruct what they have never observed during training. This inability of the generators in reconstructing anomalies is exploited in *Adversarial Generator* (Sec. 7) and intuitively confirms

our hypothesis that anomalies are treated as outliers of the data distribution (Sec. 1,4).

Fig. 6 shows a few pixel-level detections of the *Adversarial Discriminator* in different situations. In Fig. 7 we show some detection errors. Most of the errors (e.g., miss-detections) are due to the fact that the abnormal object is very small (e.g., the skateboard in the second image) or has a “normal” motion (i.e., the same speed of normally moving pedestrians in the scene). Other miss-detections are due to objects moving through a highly populated area or to severely occluded objects.

Finally, in Fig. 5 we visualize the “detection signal” on the UMN dataset using the methodology proposed in [12], in which all the scores of all the predictions in a given test frame are averaged and normalized in  $[0, 1]$ .

## 9 CONCLUSIONS

In this paper we presented a GAN-based approach for abnormality detection. We use the mutual supervisory information of the generator and the discriminator in order to train a deep network end-to-end with small weakly supervised training sets. Differently from common generation-oriented GANs, after training we directly use the discriminators as the final classifiers. In order for this approach to be effective, we designed two non-trivial cross-channel generative tasks for training our networks. As far as we know this is the first paper directly using a GAN for a discriminative task. Our results on the most common abnormality detection benchmarks show that the proposed approach largely outperforms the previous state of the art.

## REFERENCES

- [1] Thomas Brox, Andrés Bruhn, Nils Papenberg, and Joachim Weickert. 2004. High accuracy optical flow estimation based on a theory for warping. In *ECCV*.
- [2] Yang Cong, Junsong Yuan, and Ji Liu. 2011. Sparse reconstruction cost for abnormal event detection. In *CVPR*.
- [3] Ian J. Goodfellow, Jean Pouget-Abadie, Mehdi Mirza, Bing Xu, David Warde-Farley, Sherjil Ozair, Aaron C. Courville, and Yoshua Bengio. 2014. Generative Adversarial Nets. In *NIPS*.
- [4] Mahmudul Hasan, Jonghyun Choi, Jan Neumann, Amit K. Roy-Chowdhury, and Larry S. Davis. 2016. Learning Temporal Regularity in Video Sequences. In *CVPR*. 733–742.
- [5] Phillip Isola, Jun-Yan Zhu, Tinghui Zhou, and Alexei A. Efros. 2016. Image-to-Image Translation with Conditional Adversarial Networks. *arXiv:1611.07004* (2016).
- [6] Jaechul Kim and Kristen Grauman. 2009. Observe locally, infer globally: a space-time MRF for detecting abnormal activities with incremental updates. In *CVPR*.
- [7] Weixin Li, Vijay Mahadevan, and Nuno Vasconcelos. 2014. Anomaly detection and localization in crowded scenes. *PAMI* (2014).
- [8] Cewu Lu, Jianping Shi, and Jiaya Jia. 2013. Abnormal event detection at 150 fps in matlab. In *ICCV*.
- [9] Vijay Mahadevan, Weixin Li, Viral Bhalodia, and Nuno Vasconcelos. 2010. Anomaly Detection in Crowded Scenes. In *CVPR*.
- [10] Ramin Mehran, Akira Oyama, and Mubarak Shah. 2009. Abnormal crowd behavior detection using social force model. In *CVPR*.
- [11] Hossein Mousavi, Sadegh Mohammadi, Alessandro Perina, Ryad Chellali, and Vittorio Murino. 2015. Analyzing tracklets for the detection of abnormal crowd behavior. In *WACV*.
- [12] Hossein Mousavi, Moin Nabi, Hamed Kiani, Alessandro Perina, and Vittorio Murino. 2015. Crowd motion monitoring using tracklet-based commotion measure. In *ICIP*.
- [13] Anh Nguyen, Jason Yosinski, Yoshua Bengio, Alexey Dosovitskiy, and Jeff Clune. 2016. Plug and Play Generative Networks: Conditional Iterative Generation of Images in Latent Space. *arXiv preprint 1612.00005* (2016).
- [14] Alec Radford, Luke Metz, and Soumith Chintala. 2015. Unsupervised Representation Learning with Deep Convolutional Generative Adversarial Networks. *arXiv:1511.06434* (2015).
- [15] Mahdyar Ravanbakhsh, Moin Nabi, Hossein Mousavi, Enver Sangineto, and Nicu Sebe. 2016. Plug-and-play cnn for crowd motion analysis: An application in abnormal event detection. *arXiv preprint arXiv:1610.00307* (2016).
- [16] M Sabokrou, M Fathy, and M Hoseini. 2016. Video anomaly detection and localisation based on the sparsity and reconstruction error of auto-encoder. *Electronics Letters* 52, 13 (2016), 1122–1124.
- [17] Mohammad Sabokrou, Mohsen Fayyaz, Mahmood Fathy, and Reinhard Klette. 2016. Fully Convolutional Neural Network for Fast Anomaly Detection in Crowded Scenes. *arXiv preprint arXiv:1609.00866* (2016).
- [18] M. Sabokrou, M. Fayyaz, M. Fathy, and R. Klette. 2017. Deep-Cascade: Cascading 3D Deep Neural Networks for Fast Anomaly Detection and Localization in Crowded Scenes. *IEEE Transactions on Image Processing* 26, 4 (April 2017), 1992–2004. <https://doi.org/10.1109/TIP.2017.2670780>
- [19] Venkatesh Saligrama and Zhu Chen. 2012. Video anomaly detection based on local statistical aggregates. In *CVPR*.
- [20] Tim Salimans, Ian J. Goodfellow, Wojciech Zaremba, Vicki Cheung, Alec Radford, and Xi Chen. 2016. Improved Techniques for Training GANs. In *NIPS*.
- [21] Dan Xu, Yan Yan, Elisa Ricci, and Nicu Sebe. 2016. Detecting anomalous events in videos by learning deep representations of appearance and motion. *CVIU* (2016).